**EPJ manuscript No.**
(will be inserted by the editor)

# Detection of Submicron-Sized Raft-Like Domains in Membranes by Small-Angle Neutron Scattering

Jeremy Pencer[1,2,3], Thalia Mills[4], Vinicius Anghel[5], Susan Krueger[2], Richard M. Epand[6], and John Katsaras[1,7]

[1] National Research Council, Canadian Neutron Beam Centre, Chalk River Laboratories, Building 459, Station 18, Chalk River, ON, K0J 1J0, Canada
[2] NIST Center for Neutron Research, National Institute of Standards and Technology, 100 Bureau Drive, Stop 8562, Bldg 235 / Room E151, Gaithersburg, MD 20899-8562, USA
[3] Department of Physics, St. Francis Xavier University, Antigonish, NS, B2G 2W5, Canada
[4] Department of Physics and Department of Molecular Biology and Genetics, Cornell University, Ithaca, NY, 14853-2501, USA
[5] Atomic Energy of Canada Ltd., Chalk River Laboratories, Chalk River, ON, K0J 1J0, Canada
[6] Department of Biochemistry and Biomedical Sciences, McMaster University, Hamilton, Ontario L8N 3Z5, Canada
[7] Guelph-Waterloo Physics Institute and Biophysics Departmental Group, University of Guelph, Guelph, ON, N1G 2W1, Canada

Received: date / Revised version: date

**Abstract.** Using coarse grained models of heterogeneous vesicles we demonstrate the potential for small-angle neutron scattering (SANS) to detect and distinguish between two different categories of lateral segregation: 1) Unilamellar vesicles (ULV) containing a single domain and 2) the formation of several small domains or "clusters" ($\sim$ 10 nm in radius) on a ULV. Exploiting the unique sensitivity of neutron scattering to differences between hydrogen and deuterium, we show that the liquid ordered (lo) DPPC-rich phase can be selectively labeled using chain deuterated dipalymitoyl phosphatidylcholine (dDPPC), which greatly facilitates the use of SANS to detect membrane domains. SANS experiments are then performed in order to detect and characterize, on nanometer length scales, lateral heterogeneities, or so-called "rafts", in $\sim$ 30 nm radius low polydispersity ULV made up of ternary mixtures of phospholipids and cholesterol. For 1:1:1 DOPC:DPPC:cholesterol (DDC) ULV we find evidence for the formation of lateral heterogeneities on cooling below 30 °C. These heterogeneities do not appear when DOPC is replaced by SOPC. Fits to the experimental data using coarse grained models show that, at room temperature, DDC ULV each exhibit approximately 30 domains with average radii of $\sim$ 10 nm.

**PACS.** PACS-key discribing text of that key – PACS-key discribing text of that key

## 1 Introduction

In recent years, much work has been devoted to understanding the mechanisms driving lateral organization in both cell and model membranes. This interest in membrane domains is primarily driven by their potential roles in a variety of biological functions such as, immune response [1], synaptic transmission [2], intracellular trafficking [3], and as platforms for infection by viruses such as HIV [4]. While there have been many membrane domain studies carried-out over the years, presently there is continuing controversy regarding domain sizes and lifetimes [5]. Nevertheless, in the case of cell membranes, there is growing support for a model that describes rafts (functional domains) as transient clusters undergoing continual formation and dispersion, which in response to particular signals, or events, coalesce and stabilize forming much larger functional domains [5–8]. There is also a growing consensus that one of the key components of lipid rafts is cholesterol, and that membrane cholesterol levels are a determining factor in the stability and organization of these rafts [6,9].

The commonly accepted model for putative lipid rafts in vivo is of domains enriched in cholesterol and saturated sphingolipid [5]. In model membranes, ternary mixtures of cholesterol, saturated sphingolipid and unsaturated phospholipid, have been observed to separate into "raft-like" domains composed mainly of cholesterol and sphingomyelin, and non-raft domains composed primarily of unsaturated phospholipid, thus supporting the model of in vivo rafts [9]. When saturated sphingolipid is replaced by a saturated phospholipid in model systems, ternary mixtures also separate into domains enriched in cholesterol and saturated lipid and those enriched in unsaturated lipid. Consequently, the most general model of raft

*Send offprint requests to*:
J. Pencer: Jeremy.Pencer@nrc.gc.ca;
J. Katsaras: John.Katsaras@nrc.gc.ca

forming lipid mixtures, though requiring cholesterol, unsaturated and saturated lipid, may not necessarily require sphingolipid as the saturated lipid component.

An emerging picture of lipid rafts in vivo as being spatio-temporally regulated by the cell, rather than being passively formed in thermally equilibrated systems, raises the question as to the value or relevance of studies on model systems which are inherently passive and tend toward thermal equilibrium [8]. What then can studies of model systems contribute, if anything, to our understanding of domain formation in cell membranes?

Silvius [9] identifies two such categories of study for cholesterol-lipid interactions: 1) Thermodynamic and spectroscopic studies, which highlight the different interactions of various lipid species with cholesterol, contribute to our understanding of raft composition. 2) Spectroscopic and fluorescence microscopy studies, which have shown the important role that cholesterol itself plays in modulating and even promoting domain formation, contribute to our understanding of raft formation and stability.

A number of theoretical studies of model membrane systems have also proven central to elucidating the possible interactions driving lateral segregation, as well as concomitant changes to vesicle structure [10–15]. Such theoretical studies have not only helped in our understanding of possible mechanisms for cell and model membrane lateral organization, but have also motivated important experimental work on such systems. For example, the concept of and theoretical framework for domain-induced budding of membranes has been known for some time [12], but has only recently been confirmed experimentally by fluorescence microscopy studies [16].

Thus, while it is true that studies of model systems may not necessarily reveal absolute domain sizes and lifetimes comparable to those possibly found in cell membranes, these studies do provide valuable information as to the relative importance of lipids and cholesterol in stabilizing rafts and the potential impact of changes in membrane composition, or environmental variables (e.g., temperature, pH) on raft size and stability.

One of the central results from studies of laterally heterogeneous model membrane systems is the observation of lateral heterogeneities on two independent length scales. While fluorescence microscopy shows the formation of micron-sized domains (e.g. [17]), FRET and fluorescence quenching provide evidence of domains which are $< 10$ nm in diameter (e.g. [18]). Single dye fluorescence, while sensitive over all length scales to differences between the cholesterol-rich and cholesterol-depleted environments, gives indications of lateral segregation, but cannot provide information about domain sizes. Thus, the size of domains cannot be probed by fluorescence on the intermediate length scale range, between tens and hundreds of nm.

Observations of micron-sized domains have recently been used to construct phase diagrams for ternary lipid mixtures, e.g. [19–21]. The region of these phase diagrams that appears most relevant to lipid raft phenomena is the two phase or liquid-liquid coexistence region. Following the terminology initially introduced for two component lipid-sterol mixtures [22], the cholesterol-rich and cholesterol-depleted liquid phases are referred to as the liquid-ordered (lo) and liquid-disordered (ld) phases, respectively (e.g. [23]). Besides cholesterol, the lo and ld phases in ternary mixtures are typically enriched in saturated and unsaturated lipids, respectively.

The transition between the two phase region and the single fluid phase region is referred to as the "miscibility" transition by Veatch, et al. [17], and we will use the same terminology here. While the temperature and compositional boundaries for the two phase region have been defined by fluorescence microscopy and related techniques [20], there is evidence that lateral may segregation also occur above the miscibility transition [18].

As such, we propose two possible scenarios consistent with the observation of domains or rafts at two different length scales: 1) Domains in model systems vary continuously in size from nanometers up to microns. Given sufficient time at a fixed temperature, these nanometer domains will form a single, stable domain whose size is determined by the compositions of the lo and ld phases and the size of the ULV on which it resides (or system size). The upper bound domain size, in this case, is determined by the vesicle size; i.e. micron-sized vesicles will produce micron-sized domains, etc. 2) Domains are manifest as, and possibly undergo a transition between a collection of smaller length scale transient domains (which we refer to as "clusters") whose compositions differ slightly from that of the rest of the membrane, and one or several larger, stable domains. "Cluster" sizes are expected to be much smaller than and independent of system size, while stable domains are as described in the former scenario. The second scenario is proposed in analogy with the recently proposed model of rafts in cell membranes discussed by Mayor and Rao [8].

Small-angle neutron scattering (SANS) shows promise as a technique able to detect formation and characterize sizes of domains on length scales intermediate between fluorescence microscopy, FRET and fluorescence quenching techniques. SANS thus provides an opportunity to reconcile the disparate views provided by these fluorescence techniques.

The significant differences in the neutron scattering properties of hydrogen and deuterium opens the possibility for "contrast variation". By judiciously varying the $H_2O/D_2O$ ratio of the solvent it is possible to minimize the scattering from membranes of uniform composition. In the case of laterally heterogeneous membranes one can suppress the scattering contribution from any of the phases present in the membrane or choose solvent conditions which maximize the contrast between lipid phases. For example, using deuterated dipalmitoyl phosphatidylcholine (DPPC) and the appropriate solvent contrast conditions, scattering arising from heterogeneities in the membrane can be enhanced, allowing for the detection of "raft" formation. Another advantage of SANS is its sensitivity to selective deuteration of the lipid, or sterol component, a method far less likely to introduce artifacts than many others, espe-

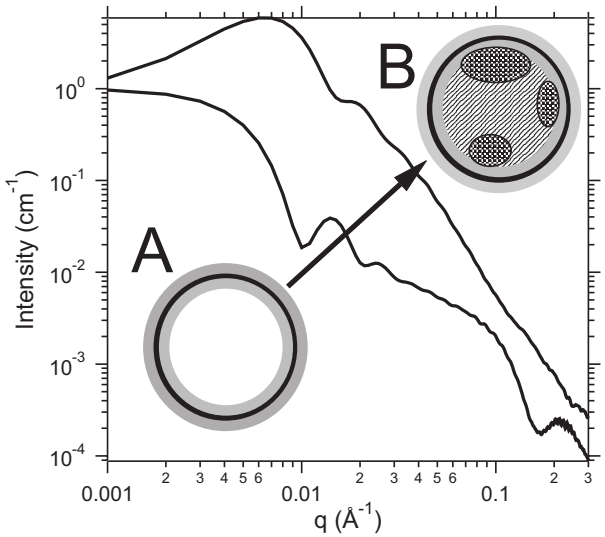


**Fig. 1.** Schematic representation of lateral segregation in a ULV as detected by SANS. A) A cartoon of a contrast matched vesicle and B) of a vesicle with laterally segregated domains. Beside each type of ULV is the expected SANS scattering curve.

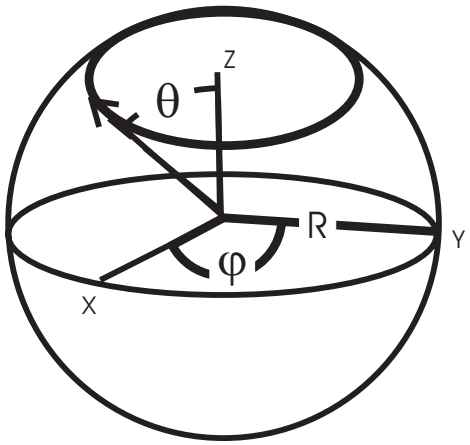


**Fig. 2.** Schematic of a ULV containing a single domain. The vesicle radius is, $R$, and the domain is defined by the bounding angle $\theta$. Also shown is the angle $\phi$.

cially compared to those which require labeling with large fluorescent moieties. Nevertheless, despite the potential of neutron scattering to characterize laterally heterogeneous membranes, such applications have been few [24,25] and have only recently been applied to ternary lipid/sterol mixtures [26].

For this study, we examine 30 nm radius ULV which, compared to larger ULV, are more amenable to SANS measurements. Restricting the system size to below 100 nm also allows us to examine whether system size and membrane curvature influence lateral segregation of ternary mixtures as compared to observations in giant unilamellar vesicles (GUV). This information is useful since vesicles used for FRET studies are likely to be closer in size to $\sim$ 100 nm radius ULV than the micron-sized GUV used in microscopy studies [18,27–29]. An additional advantage of the SANS technique to the study of ULV is that SANS provides ensemble average information by sampling a large number of vesicles (e.g. $\sim 10^{15}$ at lipid concentrations comparable to those used in this study). We should note that, while it is difficult using conventional SANS to probe length scales greater than 100's of nm, neutron experiments combining SANS with ultra SANS (USANS) could be used to study micron-sized GUV (see, e.g. [30]) typically used in fluorescence microscopy experiments.

Contrast matching gives the optimal condition for the detection of membrane domains. The 1:1:1 mixtures of DOPC : DPPC : cholesterol (DDC) and 1:1:1 mixtures of SOPC : DPPC : cholesterol (SDC) samples are prepared under contrast matching conditions at 50 °C, where it is known that lipid components are homogeneously mixed. Under these conditions, the scattering from the vesicles will be minimized. Any scattering will be the result of internal variations in scattering length density (SLD), due to differences between the acyl chain and headgroup regions (shown schematically in Fig. 1) of the lipids. When the samples are cooled, ULV exhibiting lateral segregation will show an additional contribution to the scattered intensity from the contrast between domains (also shown schematically in Fig. 1).

In order to interpret the SANS data, we investigate theoretically and by coarse grained modeling, the scattering from heterogeneous vesicles allowing us to identify features, or "signatures", in the SANS curves characteristic of vesicles containing either domains or clusters. SANS is then used to detect and characterize lateral segregation in 30 nm radius DDC ULV, a system whose mixing behavior has been well characterized by a variety of techniques [17,18,23,20,31,32]. Additionally, measurements are performed on similar ternary mixtures whereby DOPC has been replaced by SOPC (SDC).

Here, we report on the lateral segregation of lipids in DDC ULV as observed by SANS. At 20 and 25 °C, where compositions of the lo and ld phases of the DDC mixture and distribution of DPPC between the lo and ld phase are known [20], we are able to fit the SANS data extracting reasonably accurate domain sizes. Furthermore, 30 nm radius DDC ULV show domain formation over the same temperature range as observed in GUV of the same composition [20], demonstrating that neither membrane curvature nor system size appear to influence the lateral segregation taking place in these systems.

## 2 Theory

Below, we consider a general model for laterally heterogeneous ULV and show that the scattering function can be expressed as a sum of contributions corresponding to that from an equivalent homogeneous vesicle and a contribution which is due entirely to lateral heterogeneities.

### 2.1 Scattering From Laterally Heterogeneous Vesicles

The variation with $q$ of scattered intensity from a vesicle with heterogeneous SLD can be determined from [33]:

$$I(q) = \frac{16\pi^2}{q^2}\left[\frac{1}{4\pi}\int_{\boldsymbol{r}}[\rho(\boldsymbol{r})-\rho_s]\exp(\boldsymbol{q}\cdot\boldsymbol{r})d\boldsymbol{r}\right]^2, \quad (1)$$

where $\rho_s$ is the solvent SLD, and the membrane SLD, $\rho(\boldsymbol{r})$, is a function of the distance $r$ from the vesicle center. $\theta$ is the angle formed with the z-axis, while $\phi$ is the angle in the x-y plane, as shown in Fig. 2.

Expansion of $\exp(\boldsymbol{q}\cdot\boldsymbol{r})$ in spherical harmonics, makes it possible to express the orientational average of Eq. 1 in terms of a corresponding expansion in spherical Bessel functions (e.g. [33,34]) as follows

$$I(q) = 16\pi^2\left[\int_0^\infty r^2 f_{0,0}(r)j_0(qr)dr\right]^2 + \sum_{n=1}^{\infty}\left[\sum_{m=-n}^{n}16\pi^2 c_{n,m}^{-1}\left|\int_0^\infty r^2 f_{n,m}(r)j_n(qr)dr\right|^2\right], \quad (2)$$

(3)

where

$$c_{n,m} = \frac{(n+m)!}{(n-m)!}\frac{1}{2n+1} \quad (4)$$

and

$$f_{n,m} = \frac{1}{4\pi}\int_0^\pi \sin\theta P_n^m(\cos\theta) \times\left[\int_0^{2\pi}[\rho(r,\theta,\phi)-\rho_s]\exp(-im\phi)d\phi\right]d\theta. \quad (5)$$

$P_n^m(x)$ and $j_n(x)$ are the associated Legendre and spherical Bessel functions.

It is possible to express the SLD of laterally heterogeneous ULV, $\rho(\boldsymbol{r})$, as a sum of two contributions; an orientationally averaged contribution $\rho_{0,0}(r)$, given by

$$\rho_{0,0}(r) = \frac{1}{4\pi}\int_0^\pi \sin\theta\int_0^{2\pi}\rho(r,\theta,\phi)d\phi d\theta \quad (6)$$

and the component of the SLD that varies with $\theta$ and $\phi$, $\rho_f(r,\theta,\phi)$, given by

$$\rho_f(r,\theta,\phi) = \rho(r,\theta,\phi) - \rho_{0,0}(r). \quad (7)$$

Substitution of $\rho(\boldsymbol{r}) = \rho_{0,0}(r) + \rho_f(r,\theta,\phi)$ into Eq. (5) gives $f_{0,0}(r) = \rho_{0,0}(r) - \rho_s$. The scattered intensity from laterally heterogeneous vesicles can therefore be expressed as

$$I(q) = I_{0,0}(q) + I_f(q), \quad (8)$$

where $I_{0,0}(q)$ is the intensity due to the orientationally averaged SLD $\rho_{0,0}(r)$ and $I_f(q)$ is due to the fluctuations in SLD, $\rho_f(r,\theta,\phi)$, around this value. For a laterally homogeneous vesicle, $I_f(q) = 0$.

The primary goal of this study is the measurement of $I_f(q)$, corresponding to the scattering contribution from membrane domains. As will be discussed below, the relative contribution of $I_f(q)$ to $I(q)$ can be maximized by working under contrast matching conditions. However, as will be shown below, even under contrast matching conditions, $I_{0,0}(q)$ makes a nonzero contribution to the scattered intensity.

### 2.2 Scattering From Laterally Homogeneous Vesicles

For laterally homogeneous spherical vesicles, $\rho(r,\theta,\phi) = \rho_r(r)$ and Eq. (1) reduces to

$$I_{0,0}(q) = 16\pi^2\left[\int_0^\infty r^2[\rho_{0,0}(r)-\rho_s]j_0(qr)dr\right]^2. \quad (9)$$

We can define a radial averaged SLD, $\bar{\rho}$ as

$$\bar{\rho} = \frac{4\pi}{V}\int_0^\infty r^2\rho_{0,0}(r)dr \quad (10)$$

and a fluctuating radial SLD component, $\rho_r(r)$

$$\rho_r(r) = \rho_{0,0}(r) - \bar{\rho}. \quad (11)$$

The scattered intensity $I(q)$ can then be expressed as a sum of three contributions: (i) that from the radially averaged SLD, $I_{ave}(q)$. (ii) that from the radially fluctuating part of the SLD, $I_r(q)$, and (iii) an interference term $F_{ave}F_r$ as follows

$$I_{0,0}(q) = I_{ave}(q) + I_r(q) + F_{ave}F_r \quad (12)$$

The contribution to the scattered intensity from $\bar{\rho}$, $I_{ave}(q)$ is determined from the integration of Eq. (9) over a step function of thickness, $t$, and value $\bar{\rho}$ inside the membrane (and value zero outside the membrane), which gives

$$I_{ave}(q) = (\bar{\rho}-\rho_s)^2\left[R_o^3\frac{j_1(qR_o)}{qR_o} - R_i^3\frac{j_1(qR_i)}{qR_i}\right]^2, \quad (13)$$

where $R$ is the average vesicle radius, $t$ is the thickness, $R_o = R + t/2$, $Ri = R - t/2$, and $j_1(x)$ is the first-order spherical Bessel function, expressed as

$$j_1(x) = \frac{\sin(x)}{x^2} - \frac{\cos(x)}{x}. \quad (14)$$

We can determine a form for $I_r(q)$ using a multishell model for radially heterogeneous ULV. Differences between the SLD of the headgroup and acyl chain regions of the membrane, suggest a three shell model, where the innermost, central and outer shells correspond to the inner headgroup, acyl chain, and outer headgroup layers, respectively (e.g. Ref. [35]). If we assume that the SLD of each shell is uniform and that the interfaces between shells are sharp, we obtain

$$I_r(q) = \left\{\sum_{i=1}^{3}\rho_i\left[R_i^3\frac{j_1(qR_i)}{qR_i} - R_{i-1}^3\frac{j_1(qR_{i-1})}{qR_{i-1}}\right]\right\}^2, \quad (15)$$

where $R$ is the average ULV radius, and $t_t$ and $t_h$ are the thickness of the acyl chain and headgroup layers, respectively. $R_3 = R + t_h + t_t/2$, $R_2 = R + t_t/2$, $R_1 = R - t_t/2$, $R_0 = R - t_h - t_t/2$, $\rho_3 = \rho_h - \bar{\rho}$, $\rho_2 = \rho_t - \bar{\rho}$, $\rho_h$ is headgroup region SLD, $\rho_t$ is the acyl chain region SLD, and $\rho_1 = \rho_3$.

### 2.3 The Scattering Contribution From Lateral Heterogeneities

Combining Eqs. 8 and 12, we find that the scattered intensity from laterally heterogeneous vesicles can be described as a sum of four contributions: (i) the scattered intensity due to the mean SLD (averaged both radially and orientationally) $I_{ave}(q)$. (ii) the intensity due to the radially fluctuating orientational averaged SLD $I_r(q)$. (iii) an interference term between $F_{ave}(q)F_r(q)$ and finally, (iv) the laterally heterogeneous contribution of $\rho$, given by $I_f(q)$. These four contributions can be written as follows

$$I(q) = I_{ave}(q) + F_{ave}(q)F_r(q) + I_r(q) + I_f(q). \quad (16)$$

Under contrast matching conditions, $\rho_s = \bar{\rho}$, $I_{ave}(q) = 0$ and $F_{ave}(q)F_r(q) = 0$, resulting in

$$I_{match}(q) = I_r(q) + I_f(q). \quad (17)$$

Under exact contrast matching conditions, homogeneous ULV will show a scattering contribution $I_r(q)$. Thus, we should expect to see only this contribution at high temperatures. However, on cooling if lateral segregation does take place then we should expect to see an additional contribution to the scattering from $I_f(q)$ which will cause an increase in the scattered intensity at finite $q$. Prior to our discussion of experimental results, we will investigate the contribution of $I_f(q)$ relative to $I_r(q)$ using the coarse grained modeling method described below.

## 3 Experimental Procedures

### 3.1 Materials

1-stearoyl-2-oleoyl-sn-glycero-3-phosphocholine (SOPC), 1,2-dioleoyl-sn-glycero-3-phosphocholine (DOPC), 1,2-dipalmitoyl-sn-glycero-3-phosphocholine (DPPC) and 1,2-dipalmitoyl-d62-sn-glycero-3-phosphocholine (dDPPC), solubilized in chloroform, were purchased from Avanti Polar Lipids, Inc. (Birmingham, AL) and used without further purification. Upon arrival, the ampules containing the various lipids were stored at - 40 °C. Cholesterol of > 99% purity was purchased as lyophilized powder from Sigma-Aldrich (St. Louis, MO), and used without further purification. 99% purity $D_2O$ was purchased from Cambridge Scientific (Andover, MA), while all other chemicals were reagent grade. (Reference to commercial sources and products used in this study does not constitute endorsement by the National Institute of Standards and Technology (NIST), nor should it be inferred that the products mentioned are necessarily the best available for the purpose used.)

**Table 1.** Neutron scattering lengths, molecular volumes and corresponding scattering length densities of lipids and sterols used in this study. Data for $H_2O$ and $D_2O$ are also shown for comparison. $a$ = vol. at 20 °C, $b$ = vol. at 50 °C, $c$ = vol. at 30 °C, and $d$ = estimated molecular vol.

| Molecule | Chem. Formula | $b$ (fm) | $V$ (Å$^3$) | SLD (fm/Å$^3$) |
|---|---|---|---|---|
| DPPC | $C_{40}H_{80}NO_8P$ | 27.63 | 1144[a] | 0.024 |
| | | | 1232[b] | 0.022[b] |
| head | $C_{10}H_{18}NO_8P$ | 60.1 | 326[b] | 0.184 |
| chains | $C_{30}H_{62}$ | -32.4 | 891[b] | -0.036 |
| dDPPC | $C_{40}H_{18}NO_8PD_{62}$ | 672.99 | 1144[a] | 0.588 |
| | | | 1232[b] | 0.546[b] |
| head | $C_{10}H_{18}NO_8P$ | 60.1 | 326[b] | 0.184 |
| chains | $C_{30}D_{62}$ | 613 | 891[b] | 0.688 |
| DOPC | $C_{44}H_{84}NO_8P$ | 39.26 | 1303[c] | 0.030 |
| head | $C_{10}H_{18}NO_8P$ | 60.1 | 337[b] | 0.178 |
| chains | $C_{34}H_{66}$ | -13.3 | 981[b] | -0.014 |
| SOPC | $C_{44}H_{86}NO_8P$ | 31.78 | 1303[d] | 0.024 |
| head | $C_{10}H_{18}NO_8P$ | 60.1 | 337[b] | 0.178 |
| chains | $C_{34}H_{68}$ | -19.1 | 963[b] | -0.020 |
| Chol. | $C_{27}H_{46}O$ | 13.25 | 629 | 0.021 |
| Water | $H_2O$ | -1.68 | 30 | -0.056 |
| Heavy Water | $D_2O$ | 19.15 | 29.9 | 0.64 |

### 3.2 Vesicle Preparation

30 nm radius ULV were prepared by extrusion using the method of Nayar, et al. [36]. Lipids solubilized in chloroform were transferred to round bottom flasks and the chloroform was removed under a stream of $N_2$ followed by vacuum pumping. Vacuum pumping was performed with lipid films at $\sim$ 60 °C to ensure that mixtures did not phase separate during solvent removal. Lipid films were then dispersed, by agitation, into deionized water that was filtered using a Millipore Milli-Q water purification system (mixed in appropriate proportions with $D_2O$), which had also been preheated to 60 °C. The lipid dispersions were then extruded using a device described in Refs. [36,37]. The extruder was preheated to 60 °C and pressurized to $\sim$ 700 kPa using $N_2$. Total lipid concentrations ranged from 1 to 10 mg/ml. 30 nm radius ULV were formed by successive extrusions using three different pore diameter polycarbonate filters and a total of 27 passes [e.g., 200-nm (9 times), 100-nm (9 times) and 50-nm (19 times)].

### 3.3 Small-Angle Neutron Scattering

SANS measurements were performed using the 30 m NG7 instrument [38] located at NIST (Gaithersburg, MD). 1.5 and 12 m sample-to-detector distances (SDD) were used along with a neutron wavelength, $\lambda$, of 8 Å ($\delta\lambda/\lambda = 10\%$), resulting in a total range in scattering vector, $q = 4\pi \sin(\theta/2)/\lambda$, of $0.004 < q < 0.3$ Å$^{-1}$. Additional measurements were performed on the NG1 8 m SANS using an SDD of 3.84

m and $\lambda = 6$ and 10 Å ($\delta\lambda/\lambda = 12\%$), resulting in a total range in q of $0.006 < q < 0.18$ Å$^{-1}$.

In order to account for vesicle polydispersity, the scattering function is integrated over the Schulz, or Gamma distribution given by

$$G(R) = \left(\frac{m+1}{R_a}\right)^{m+1} \frac{R^m}{\Gamma(m+1)} \exp\left(\frac{-R(m+1)}{R_a}\right), \quad (18)$$

where the number average vesicle radius is equal to $R_a$, the variance is $\sigma^2 = R_a^2/(m+1)$ and the polydispersity (relative variance) is $\Delta^2 = 1/(m+1)$. Data were also corrected for instrumental resolution, as discussed in [38]. As discussed in Ref [39], detailed information in the scattering function related to the membrane SLD profile appears above roughly $q = 0.05$ Å$^{-1}$ and is difficult to distinguish because of the large contribution to scattering from the incoherent background. As such, SANS data collected for homogeneous vesicles were fit using the form factor given by equation (13), where the thickness determined corresonds to an average weighted by the SLD profile of the membrane. Fits to scattering curves from heterogeneous vesicles were performed using the modeling procedure described below and in tandem with the program OLIGOMER [40].

### 3.4 Contrast Matching of Homogeneous Vesicles

ULV used in SANS measurements were prepared in $H_2O/D_2O$ mixtures and, unless specified otherwise, in proportions expected to produce contrast matching conditions when the lipids are homogeneously mixed, which we assume takes place on heating above 50 °C. For contrast matching condition of binary 1:1 mixtures of deuterated DPPC (dDPPC) and hydrogenous DPPC, we used 49 % $D_2O$ by volume, while for ternary 1:1:1 mixtures of DOPC: dDPPC : cholesterol and SOPC : dDPPC : cholesterol, we used 40 % $D_2O$. Contrast matching conditions were determined from known nuclear scattering lengths [41] and the molecular volumes of DOPC, DPPC [42] and cholesterol [43], as shown below. Table 1 shows scattering lengths, molecular volumes (or estimated molecular volumes) and SLD of the lipids used in this study, as well as those of light ($H_2O$) and heavy ($D_2O$) water. These parameters are also given for the lipid components, denoted "head" and "chain". Here, the lipid "head" is composed of the choline, phosphate, glycerol and two carbonyl groups, while the lipid "chains" contain the remaining $CH_2$ and $CH_3$ groups in the acyl chains.

The SLD of lo and ld phases, as well as homogeneous mixtures, can be expressed as

$$\rho_i = \frac{xa_i b_a + xb_i b_b + xc_i b_c}{xa_i Va_i + xb_i Vb_i + xc_i Vc_i}, \quad (19)$$

where $i = 1, 2$, $\rho_i$ is the SLD of phase $i$, and $xa_i$, $xb_i$, $xc_i$ are the mole fractions of components a, b, and c in phase $i$, respectively. $b_a$, $b_b$ and $b_c$ are the scattering lengths of components $a$, $b$ and $c$, and $Va_i$, $Vb_i$ and $Vc_i$ are the molecular volumes of $a$, $b$ and $c$, respectively, in phase $i$. Equation 1 can also be used to evaluate the SLD for the case where all three components are mixed homogeneously into a single phase $i$. Here, we assume that the volume of each component is the same in both the lo and ld phases. To verify this assumption, we have calculated and compared SLD of ternary mixtures containing dDPPC using the volume of DPPC either in the gel or fluid phase. We find, that in all cases the resulting differences are less than $\sim 1\%$.

**Table 2.** SLD and corresponding contrast match points for lipid/sterol mixtures, as determined using Eq. (2), and scattering lengths and volumes from Table 1. Values are determined from the molecular volume of DPPC in the fluid phase (i.e. at 50°C).

| Mixture | SLD (fm/Å$^3$) | Match Point (% $D_2O$) |
|---|---|---|
| 1:1:1 DPPC/DOPC/chol | 0.025 | 12.0 |
| 1:1:1 dDPPC/DOPC/chol | 0.229 | 41.1 |
| 1:1:1 dDPPC/SOPC/chol | 0.227 | 40.8 |
| 1:1 dDPPC/DPPC | 0.285 | 49.0 |
| 1:1 DPPC/chol | 0.022 | 11.0 |
| 1:1 dDPPC/chol | 0.369 | 61.2 |
| lo phase, 0.53:0.05:0.42 dDPPC/DOPC/chol | 0.375 | 61.8 |
| ld phase, 0.18:0.60:0.22 dDPPC/DOPC/chol | 0.130 | 26.8 |

Summarized in Table 2 are the calculated SLD for uniform DDC and SDC. These SLD were calculated from the scattering lengths and molecular volumes of the individual components given in Table 1. For comparison, we also determine the SLD for phases composed of 1:1 DPPC:cholesterol, 1:1 dDPPC:cholesterol and for the lo and ld phases of 1:1:1 mixtures of DOPC:DPPC:cholesterol using the phase compositions estimated in [20] at 25 °C. Contrast match points are determined for the various mixtures and written as a percentage of $D_2O$, in an $H_2O$ / $D_2O$ mixture.

### 3.5 Modeling of SANS Data

SANS profiles from homogeneous and heterogeneous vesicles are calculated using a modified coarse graining method as described in [44,45]. Briefly, a vesicle is coarse grained via the replacement of atoms in the scattering volume with a fixed number of uniformly-sized beads whose SLD correspond to the appropriate lipids, or collections of lipids. Beads are randomly placed within the scattering volume using a pseudo-random number generator which is used to calculate the coordinates of the beads. These beads, and their corresponding SLD, are then used to generate an SLD weighted distance distribution function, $p(r)$, which in turn is used to calculate the orientationally averaged scattered intensity. Because this method uses a pseudo-random number generator, it is often referred to as a "Monte Carlo" method. However, it should not be con-

fused with commonly used "Monte Carlo simulations", where similar random number generators are used to construct ensembles of particles for the purpose of simulating particle interactions and calculating thermodynamic quantities [46].

### 3.6 Measurements of Lateral Segregation

The detection of lateral segregation using SANS relies on the use of a deuterated component and medium compositions that contrast match the mean SLD of the ULV. At high temperatures, when the lipid components are expected to be homogeneously mixed, contrast matching conditions result in a significant reduction in scattered intensity. In particular, the only scattering under these conditions will result from differences between the SLD of the lipid's acyl chains and headgroup. As the vesicles are cooled, if lateral segregation occurs, the SLD of the segregated phases will deviate significantly from that of the surrounding medium, resulting in an excess of scattering compared to contrast matched vesicles (Fig. 1).

### 3.7 Characterization of Vesicle Stability

To measure ULV size and polydispersity, vesicles were also characterized under high contrast conditions at 70 and 100 % $D_2O$ content. Measurements were taken at 50 °C before and after cooling sequences. In order to characterize vesicles away from contrast matching conditions, contrast matched samples were diluted into equal volumes of $D_2O$, yielding a final $D_2O$ concentration of 70%. The data were fit using the form factor for homogeneous vesicles, the Schulz distribution to describe ULV polydispersity (e.g. [47]) and a Gaussian approximation to the instrumental resolution (e.g. [38,48]).

## 4 Results and Discussion

### 4.1 Modelling

As mentioned previously, a coarse graining method is used to determine lateral segregation from SANS data. When two phases (lo and ld) coexist we assume, that the boundaries between these two phases are sharp, or, in other words, that the composition within each phase does not vary. While such an assumption may constitute an oversimplification, we feel justified in making it, since it would appear consistent with observations elsewhere, e.g. [31, 20]. In this case, the SLD is $\rho(r,\theta,\phi) = \rho_1$ for phase 1 and $\rho(r,\theta,\phi) = \rho_2$ for phase 2. As in the case with laterally homogeneous membranes, the variation of $\rho$ with $r$ is related to the membrane bilayer structure, which will have two forms corresponding to the density profiles of phase 1 and 2, $\rho_1(r)$ and $\rho_2(r)$, respectively. Based on the observations of Gandhavadi, et al. [49], we take the thickness of the acyl chain region for the lo phase to be 40 Å and 30 Å for the ld phase. For both phases, we assume that the thickness of the headgroup regions are the same, 5 Å.

**Table 3.** Parameters used for the calculation of scattering models depicted in Fig. 3. $x$ is the fraction of total DPPC in the lo phase, $a_0$ is the relative area of the lo phase and $r$ is the domain radius. comp. refers to the composition of the ld or lo phase as the molar ratio DOPC:DPPC:cholesterol, and $\Delta\rho$ is the SLD contrast of the acyl chain region (ACR) of either the lo or ld phase. For both phases, the SLD contrast of the headgroup region is -0.047.

| $1-x$ | $a_0$ | $r$ (Å) | comp. | $\Delta\rho$ ACR (fm/Å$^3$) |
|---|---|---|---|---|
| ld phase | | | | |
| 0.8 | 0.12 | 225 | 37:31:32 | 0 |
| 0.6 | 0.24 | 318 | 43:27:30 | -0.033 |
| 0.4 | 0.36 | 390 | 51:21:28 | -0.079 |
| 0.2 | 0.48 | 450 | 62:13:25 | -0.140 |
| 0.0 | 0.60 | 503 | 81:0:19 | -0.216 |
| lo phase | | | | |
| n/a | n/a | n/a | 5:53:42 | 0.195 |

In order to calculate model scattering curves, we use the composition of the lo phase at 20 °C, having the ratio DOPC : DPPC : cholesterol = 5:53:42 [20], and assume that this composition does not depend on domain size. Calculations are performed for ULV under near contrast matching conditions, corresponding to a 40 % $D_2O$ concentration in the medium. In order to vary the domain size, we use the distribution of DPPC between the lo and ld phase as a free parameter. Since the composition of the lo phase is fixed, and the total amount of each component is also fixed, the composition of the ld phase is then set by this distribution. In particular, if x is the relative amount of DPPC in the lo phase, for a 1:1:1 mixture, the composition of the ld phase is then given by

$$\text{DOPC:DPPC:cholesterol} = \left(1-\frac{5}{53}\right)x : (1-x) : \left(1-\frac{42}{53}\right)x. \quad (20)$$

To estimate the relative areas of the lo and ld phases, we assume that the cross sectional areas of the lipid and sterol components are the same in these two phases and that the cross sectional areas of DOPC and DPPC are equal, and twice that of cholesterol. We then use the parameter $a_0$ to denote the area of the lo phase relative to that of the total vesicle area. The SLD for the acyl chain and headgroup regions are given in Table 3 for several compositions of the ld phase.

We can define a single circular domain with SLD, $\rho_2$, by setting $\rho(\theta,\phi) = \rho_2$ for $\theta < \theta_c$ and $\rho(\theta,\phi) = \rho_1$ for $\theta \geq \theta_c$, and consider domain sizes between $0 \leq \theta_c \leq \pi/2$. $\theta_c = 0$ to correspond to homogeneous ULV and $\theta_c = \pi/2$ describing a domain which makes up half the ULV surface. A domain bounded by $\theta_c$ on a ULV of radius $R$ will have an area, $A$, given by

$$A = 2\pi R^2(1-\cos\theta_c). \quad (21)$$

We define a reduced area, $a_0$ to be the area fraction occupied by the lo phase. In the case where this phase is

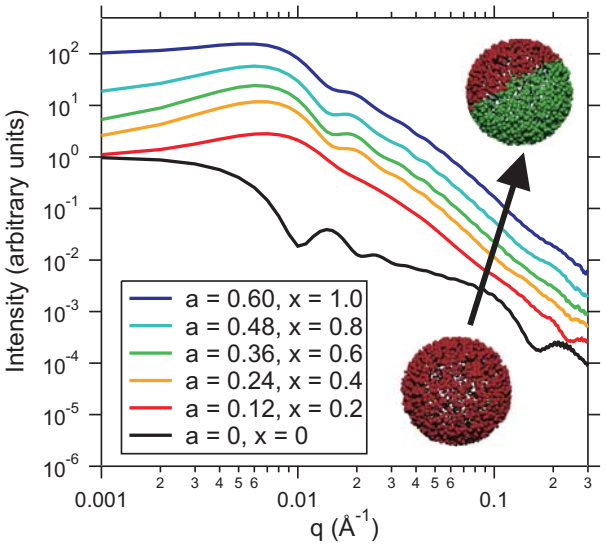


**Fig. 3.** Predicted scattering profiles from polydisperse ULV with single domains. Curves are shifted on the vertical axis to facilitate viewing. The domain sizes increase on going from the bottom to the top curves.

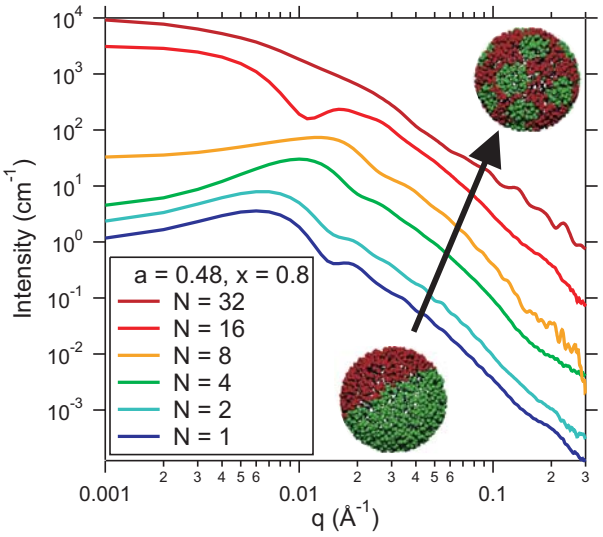


**Fig. 4.** Predicted scattering from polydisperse ULV containing multiple domains. The number of domains increases on going from the bottom to the top curves. Curves are shifted on the vertical axis to facilitate viewing.

entirely found in a single domain, the reduced area is then

$$a_0 = \frac{1}{2}(1 - \cos\theta_c). \tag{22}$$

A single domain of radius $r$ then has an area, $A = \pi r^2$, which results in

$$r = R\sqrt{2(1 - \cos\theta_c)}. \tag{23}$$

It should be noted that, given the definition of domain radius, $r$, which is determined by the vesicle surface area, $r$ can achieve values greater than the vesicle radius, $R$; e.g., when a domain occupies half the vesicle surface, $r = \sqrt{2}R$, and when the domain occupies the entire vesicle, $r$ has a maximum value of $2R$.

Figure 3 depicts calculated SANS curves from polydisperse ULV containing variable size, single domains. Parameters used for these models are summarized in Table 3. Homogeneous vesicles at near contrast matched conditions show a scattering curve that appears qualitatively similar to that seen for the ULV under high contrast conditions (e.g. ULV in 60 % $D_2O$, as shown in Fig. 6 below). ULV containing single domains, however, show a positive slope at low $q$. This positive slope reflects the contributions of the non-zero order spherical Bessel functions, which become significant when lateral heterogeneities appear. The domain size in heterogeneous ULV does not appear to influence the $q$ position of the scattering minimum, but does influence the overall shape of the scattering curves.

For vesicles with N clusters, we assume that all clusters on the ULV are identical, having a relative area $a_0/N$, are placed at random locations on the ULV surface, and do not overlap. In this case, the radius, $r_N$ of the domains can be related to that of a single domain of radius $r_1$, enclosing the same area, as $r_N = r_1/\sqrt{N}$. In order to account for the different possible relative arrangements of the clusters, scattering curves for vesicles are averaged over at least 50 different configurations.

Figure 4 depicts scattering curves for ULV with multiple domains, ranging in number from 1 to 32. For this set of models, the composition and total area of the lo phase are fixed, corresponding to $x = 0.8$ and $a_0 = 0.48$, respectively.

When the number of domains is below $\sim$ 10 the scattering curves of ULV with multiple clusters appear qualitatively similar to those for single domains. These curves show a positive slope at low $q$, followed by a peak at intermediate $q$ and then a small scattering minimum at a slightly higher $q$. The scattering peak and subsequent minimum shift to higher $q$ values as the number of domains increases. This behavior suggests that the $q$ positions of the scattering maxima and subsequent minima may be correlated to the domain size; as the domains get smaller, the scattering contribution moves to shorter length scales, or larger $q$. For ULV having more than $\sim$ 10 domains, the scattering function shows a negative slope at low $q$. This negative slope likely reflects the underlying contribution to the scattering function from the homogeneous ULV contribution $I_{0,0}(q)$, which could begin to dominate the scattering function as the contribution from heterogeneities shifts to sufficiently high $q$.

### 4.2 Vesicle Size, Polydispersity and Stability

In order to verify the stability of extruded vesicles through the miscibility transition, we performed measurements on DDC ULV containing protonated DPPC in 40 % $D_2O$. At these contrast conditions, the homogeneous part of the form factor dominates over the heterogeneous parts. Scattering curves measured at 25 and 50 °C are shown in Fig. 5, along with temperature dependent changes in vesi-

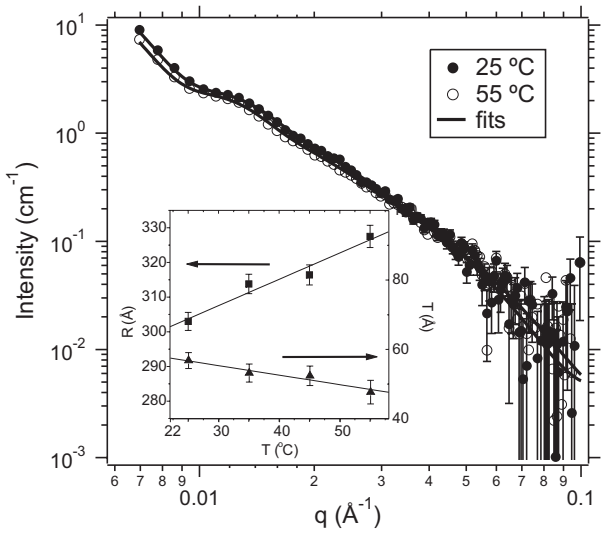


**Fig. 5.** SANS measurements of protonated DDC ULV measured at 25 and 55 °C, both in 40 % $D_2O$. The inset to the figure shows the vesicle radius as a function of increasing temperature.

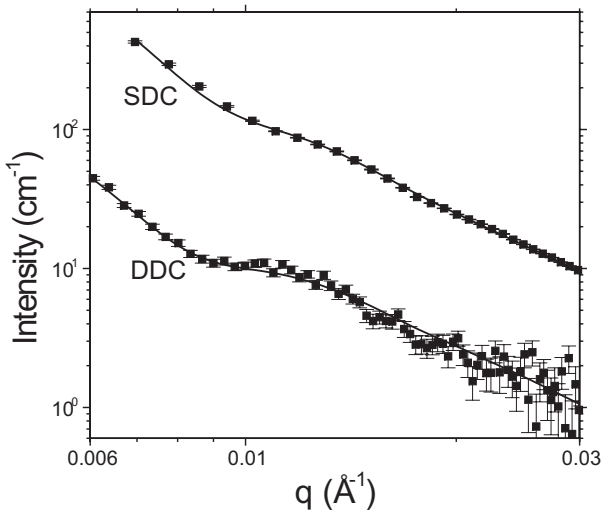


**Fig. 6.** Neutron scattering from 30 nm radius DDC and SDC ULV, in 70 and 100 % $D_2O$, respectively. Fits to the data are shown as solid lines.

cle size and membrane thickness (inset to Fig. 5). Over the entire temperature range, fits to the data show that the DDC ULV are spherical with a low polydispersity, $0.26 \pm 0.01$, which is temperature independent. On heating from 25 to 50 °C, ULV size increases, while membrane thickness decreases.

We also performed measurements on ULV containing deuterated DPPC after temperature cycling between 50 and 5 °C. Figure 6 depicts scattering data for DDC and SDC mixtures, along with fits to the data. We find that for each mixture, temperature cycling has not disturbed the overall vesicular structure and differences in composition do not appear to make a significant impact on ULV size or polydispersity. The mean radii of these vesicles are $327.8 \pm 2.8$ and $314.2 \pm 1.5$ Å for DDC and SDC ULV mixtures, respectively. The thicknesses are $54.3 \pm 0.8$ and $53.0 \pm 0.9$ and corresponding polydispersities (relative standard deviation, $\sigma / < R >$) were both $0.26 \pm 0.01$ (error bars correspond to the error in the fit to the data).

### 4.3 Lateral Segregation

In Figures 7 and 8 SANS scattering data are shown for ULV composed of DDC and SDC, respectively, in 40 % $D_2O$, near the contrast match conditions for both mixtures. The scattered intensity is plotted on a linear scale in the inset of each plot, with a larger plot showing the intensity on a log scale. The data in each case are plotted on an absolute scale. Figure 9 shows similar plots for a 1:1 mixture of dDPPC and DPPC.

The scattering observed at 50 °C is most likely the result of the difference between the SLD of the acyl chain and headgroup regions (as discussed above). On cooling from 30 to 25 °C, the DDC sample shows significant increases in scattered intensity at low and intermediate $q$, while the SDC sample does not. Results for the DDC sample could be due to changes in the differences between the acyl chain and headgroup regions, such as those due to changes in the density of the acyl chain region, e.g. arising from the gel-fluid phase transition of a pure lipid membrane. Since our measurements on 1:1 dDPPC/DPPC show no such change, we dismiss this possibility. Alternatively, our observations could be due to changes in ULV shape. This possibility can also be discounted, since no changes to vesicle shape are observed for the DDC samples with hydrogenous DPPC over the same temperature range.

The most likely explanation for the observed behaviour of the DDC sample is the formation of domains which is consistent with the observation of a miscibility transition between 25 and 30 °C for DDC. Interestingly, the temperature range where we observe evidence for lateral segregation corresponds to the two phase region identified by Veatch, et al. [20]. Below, we use our coarse grained models to provide a quantitative interpretation of the results for the DDC mixtures.

### 4.4 Characterization of Domains

The compositions of lo and ld phases are known for 1:1:1 mixtures of DDC at 20 and 25 °C [20]. We can therefore, calculate the SLD and respective areas of these phases at these two temperatures, thus allowing us to directly compare our experimental scattering data with the models discussed in the Theory section. Table 4 shows the compositions and corresponding SLD of the lo and ld phases in DDC at 20 and 25 °C. The data are best fit using a mean radius and polydispersity of 324.5 Å and 0.17, respectively. The results presented here correspond to fits using these values.

Since the compositions of the lo and ld phases are fixed, the amounts of each component and total area of the lo phase are then, also fixed. Thus the only free parameter for fitting the scattering data is the number of domains or

**Table 4.** Parameters used for the calculation of scattering models. These models were used to fit the data in Figs. 10 and 11. $x$ is the fraction of total DPPC in the lo phase, $a_0$ is the relative area of the lo phase, $\rho_{lo}$ and $\rho_{ld}$ are the SLD of the acyl chain regions of the lo and ld phases, respectively, while $\Delta\rho_{lo}$ and $\Delta\rho_{ld}$ are the corresponding SLD contrasts in 40 % D2O. Compositions of the lo and ld phases at 20 and 25 °C are taken from [20]

| T (°C) | $x$ | $a_0$ | lo comp. | ld comp. | $\rho_{lo}$ (fm/Å$^3$) | $\rho_{ld}$ (fm/Å$^3$) | $\Delta\rho_{lo}$ (fm/Å$^3$) | $\Delta\rho_{ld}$(fm/Å$^3$) |
|---|---|---|---|---|---|---|---|---|
| 20 | 0.75 | 0.45 | 5:53:42 | 59:14:27 | 0.423 | 0.093 | 0.203 | -0.127 |
| 25 | 0.70 | 0.40 | 5:53:42 | 60:18:22 | 0.423 | 0.119 | 0.203 | -0.101 |

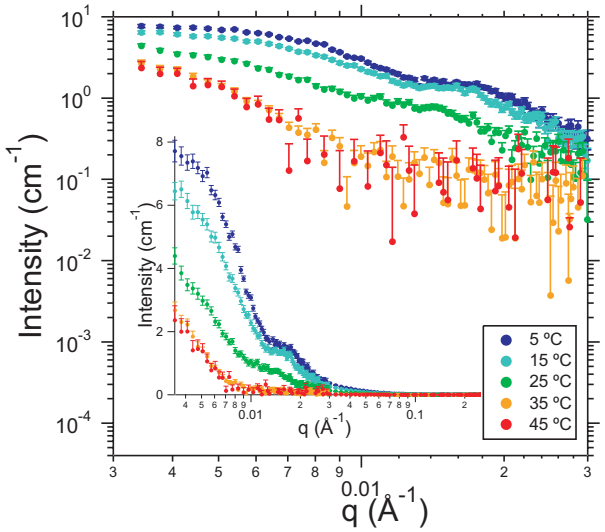


**Fig. 7.** Small angle scattering from 30 nm radius DDC ULV, with chain deuterated DPPC, in 40 % $D_2O$. The inset shows the full range of scattering data while the low angle region is shown expanded in the main plot.

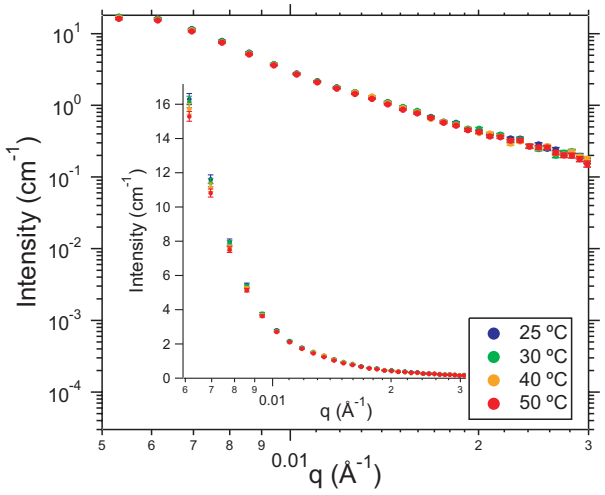


**Fig. 8.** Small angle scattering from 30 nm radius SDC ULV, with chain deuterated DPPC, in 40 % $D_2O$. The inset shows the full range of scattering data while the low angle region is shown expanded in the main plot.

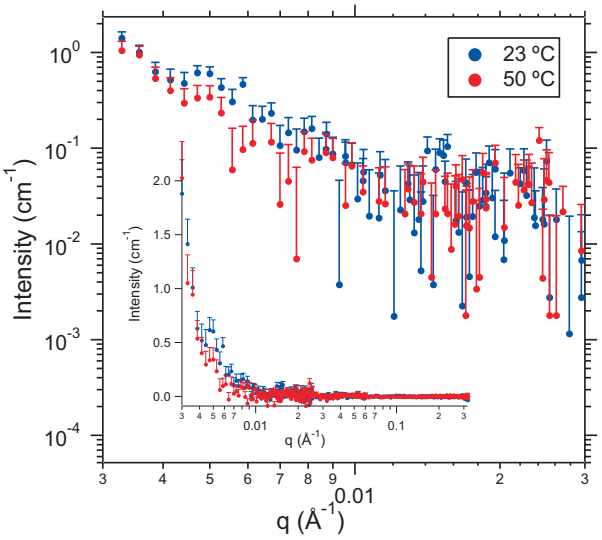


**Fig. 9.** Small angle scattering from 30 nm radius 1:1 dDPPC/DPPC ULV, in 49 % $D_2O$. The inset shows the full range of scattering data while the low angle region is shown expanded in the main plot.

clusters making up the lo phase. In order to fit the data from DDC ULV at 20 and 25 °C we systematically vary the number of domains per vesicle from 1 to 32, observing the constraints that the total area of the lo phase, and its composition (therefore SLD), remain fixed. We also consider the situation where samples may contain a mixture of ULV with varying number of domains.

Figs. 10 and 11 show the best fits to the data for 20 and 25 °C ULV. At 20 °C, nearly 95 % of the ULV contain ∼ 30 domains of radius 80 Å, while the remaining ULV have either one or ∼ 8 domains of radii ∼ 400 or 140 Å, respectively. At 25 °C, the vesicle fractions are again ∼ 95 % ULV, with approximately 30 domains of radius 70 Å, and the remaining ULV with approximately 6 domains each of size ∼ 150 Å.

At both 20 and 25 °C, we observe that the majority of ULV show a large number of lo domains surrounded by the ld phase, which makes up the remaining ULV surface. Based on the observations of Veatch and Keller [17], we would have expected the domains to coalesce over the time scale of our measurements. However, in certain cases, such as when the areas of the lo and ld phases are comparable in size, Veatch and Keller [17] have also observed that small domains can become kinetically trapped in a larger domain of the opposite phase. While we have allowed sam-

ples to equilibrate for at least 30 minutes prior to each measurement, the actual cooling rate of $\sim 5$ °C/min between measurements may have led to the presence of kinetically trapped domains.

Because we know the exact compositions of the lo and ld phases of DDC ULV at 20 and 25 °C, we have been able to predict the number of domains and their size. However, such detailed analysis of the data is not possible at the other temperatures, since the compositions of the lo and ld phases are not known. For DDC mixtures at 30 °C or above (Fig. 7), we see no evidence of lateral segregation. Cooling below 25 °C, however, leads to further increases in the absolute scattered intensity at finite $q$.

For data between 5 and 25 °C, the appearance of a broad peak in the scattered intensity at intermediate $q$ and a negative slope at low $q$ are suggestive of the presence of a large number of domains per ULV. However, since our fits at 20 and 25 °C show populations of ULV containing either one or several domains coexisting, potentially, with ULV having a large number (i.e. $> 30$) of domains, we cannot discount the presence of ULV, at lower temperatures, containing a few domains.

As previously discussed, we see no change in either the scattered intensity or angle dependent scattering for SDC mixtures (Fig. 8), clearly demonstrating that lateral segregation does not occur for this system in the temperature range examined.

In contrast to FRET studies, which report nanometer length scale heterogeneities at 37 °C we do not observe domain formation near that temperature in DDC ULV. This discrepancy between our results and those obtained by FRET is somewhat unexpected, as we are able to observe small ($\sim 10$ nm) radius domains in low temperature DDC ULV. This would seem to indicate that, either there is no lateral segregation above the liquidus boundary or miscibility transition, or that heterogeneities appearing at temperatures outside the two phase region are either too small (i.e. composed of only a few lipids) or have too little contrast with the rest of the membrane, to be detected by SANS.

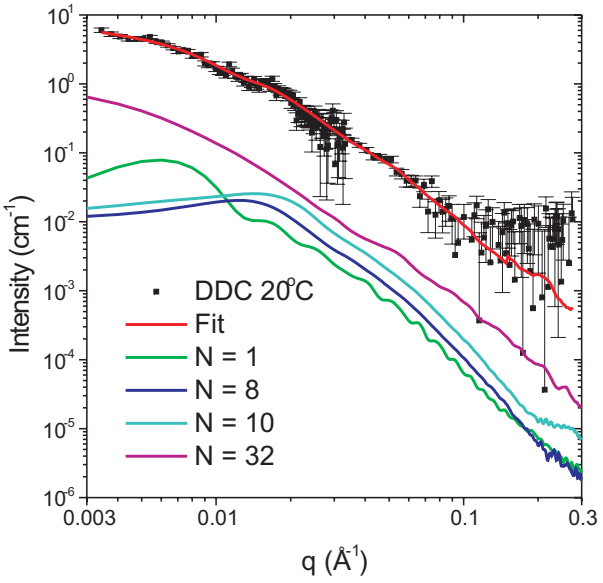


**Fig. 10.** Small-angle neutron scattering from DDC ULV at 20 °C and fit to the data corresponding to a superposition of signals from vesicles with single and multiple domains. Also shown are the individual curves that compose the fit, shifted on the vertical axis.

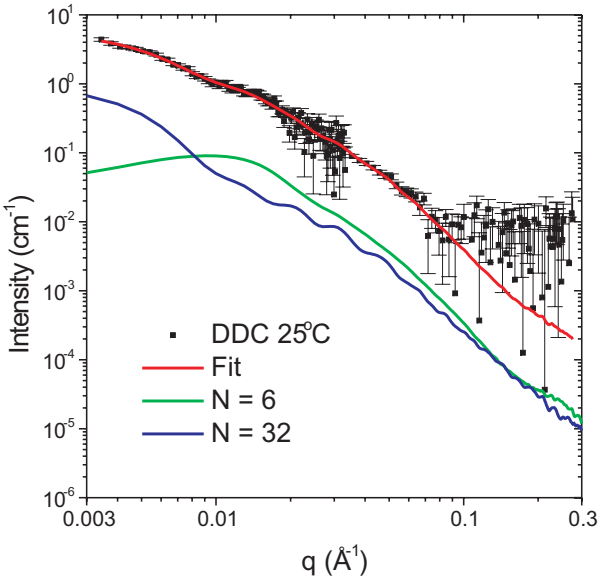


**Fig. 11.** Small-angle neutron scattering from DDC ULV at 25 °C and fit to the data corresponding to a superposition of signals from vesicles with single and multiple domains. Also shown are the individual curves that compose the fit, shifted on the vertical axis.

## 5 Conclusions

Using SANS, we have shown evidence for lateral segregation in ULV of so-called "raft" forming lipid mixtures. More importantly, we have demonstrated the ability of SANS to distinguish between the formation of single domains, of the order of the size of the ULV, and smaller, multiple clusters. Formation of dDPPC-rich domains is clearly seen in DOPC : dDPPC : cholesterol mixtures, while no such observation is made when DOPC is substituted with SOPC. In the case of DDC mixtures, the miscibility transition and macroscopic phase separation occur at the same temperature and over the same temperature range as observed by fluorescence microscopy, demonstrating that neither vesicle size nor curvature greatly modify domain formation in these membranes.

While our findings regarding domain formation in ULV are unambiguous, detailed knowledge of the phase diagrams is required in order to quantitatively interpret SANS data using coarse grained models. Here, we have determined the sizes and numbers of domains present for DDC ULV at 20 and 25 °C, where such information was available.

For certain cases (e.g. one domain per ULV), it is possible to derive analytic models for scattering from heterogeneous ULV. We are currently developing a series of

such models in order to develop a fitting method which does not require a priori knowledge of domain composition. Concomitant to this work, we are also investigating ULV of varying size and a wider range of membrane compositions in order to further study the influence of membrane curvature and the architecture of lipids and sterols on membrane lateral organization. We hope that the present results may stimulate work complementary to SANS, in determining the behaviour of ternary lipid-sterol mixtures and their phase diagrams, as well as the broader application of SANS to study lateral organization in model membranes.

The authors thank T. Harroun, L. Porcar, J. C. Shillcock, R. Dimova, R. Winter, G. W. Feigenson and the members of the CNBT research partnership for valuable discussions and D. Ho, J. Krzywon, and B. Greenwald for assistance with SANS measurements. JP is grateful to Avanti Polar Lipids for their assistance and in particular their willingness and ability to provide materials on very short notice, M. Paulaitis for support during portions of this study and R. Lipowsky for suggesting some aspects of this problem and fruitful discussions. We acknowledge the support of the National Institute of Standards and Technology, U.S. Department of Commerce, in providing the neutron research facilities used in this work and The Advanced Foods and Materials Network (Networks of Centres of Excellence, Canada) for financial assistance. This study was also performed with support from the National Institutes of Health grant no. 1 R01 RR14812 and the Regents of the University of California through contributions from the Cold Neutrons for Biology and Technology (CNBT) research partnership. JP was also supported in part through NIST grant 60-B1D0055, "Development of a Broader User Base in Small Angle Neutron Scattering Research on Molecules of Biological Relevance". Portions of this work were also supported by CIHR grant MA-7654, held by RME.

## References

1. Simons, K. and Toomre, D., Nat. Rev. Mol. Cell Biol. **1**, (2000) 31-41.
2. Tsui-Pierchala, B. A., Encinas, M., Milbrandt, J., and Johnson, E. M. Jr., Trends Neurosci. **25**, (2002) 412-417.
3. Brown, D. A., and London, E., Annu. Rev. Cell Dev. Biol. **14**, (1998) 111-136.
4. Ono, A. and Freed, E. O., Proc. Natl. Acad. Sci., **98**, (2001) 13925-13930.
5. Simons, K. and Vaz, W. L. C., Annu. Rev. Biophys. Biomol. Struct., **33**, (2004) 269-295.
6. Edidin, M. Annu. Rev. Biophys. Biomol. Struct. **32**, (2003) 257-283.
7. Subczynski, W. K. and Kusumi, A., Biochim. Biophys. Acta. **1610**, (2003) 231243.
8. Mayor, S. and Rao, M., Traffic, **5**, (2004) 231-240.
9. Silvius, J. R., Biochim. Biophys. Acta. **1620**, (2003) 174-183.
10. Lipowsky, R. J. Phys. II France, **2**, (1992) 1825-1840.
11. Kumar, P. B. S., Gompper, G., and Lipowsky, R., Phys. Rev. Lett., **86**, (2001) 3911-3914.
12. Lipowsky, R. and Dimova, R., J. Phys. Cond. Matt., **15**, (2003) S31-S45.
13. Yamamoto, S. and Hyodo, S., J. Chem. Phys., **118** (2003) 7937-7943.
14. Pandit, S. A., Jakobsson, E. and Scott, H. L., Biophys. J., **87** (2004) 3312-3322.
15. Zuckermann, M. J., Ipsen, J. H., Miao, L., Mouritsen, O. G., Nielsen, M., Polson, J., Thewalt, J., Vattulainen, I., Zhu, H., Methods Enzymol., **383** (2004) 198-229.
16. Baumgart, T., Hess, S. T. and Webb, W. W., Nature, **425** (2003) 821-824.
17. Veatch, S. L. and Keller, S. L., Biophys. J., **85**, (2003) 3074-3083.
18. Silvius, J. R., Biophys. J., **85**, (2003) 1034-1045.
19. Feigenson, G. W. and Buboltz, J. T., Biophys. J. **80**, (2001) 27752788.
20. Veatch, S.L., Polozov, I. V., Gawrisch, K. and Keller, S. L., Biophys. J., **86**, (2004) 29102922.
21. Veatch, S.L., and Keller, S.L., Biochim. Biophys. Acta. *in press* (2005).
22. Vist, M. R. and Davis, J. H. Biochemistry, **29**, (1990) 451-464.
23. Dietrich, C., Bagatolli, L. A., Volovyk, Z. N., Thompson, N. L., Levi, M., Jacobson, K., and Gratton, E., Biophys. J., **80**, (2001) 1417-1428.
24. Knoll, W., Schmidt, G., Rtzer, H., Henkel, T., Pfeiffer, W., Sackmann, E., Mittler-Neher, S., and Spinke, J., Chem. Phys. Lipids **57**, (1991) 363-374.
25. Fahsel, S., Pospiech, E.-M., Zein, M., Hazlet, T. L., Gratton, E., and Winter, R., Biophys. J. **83**, (2002) 334-344.
26. Nicolini, C., Thiyagarajan, P., and Winter, R., Phys. Chem. Chem. Phys., **6**, (2004) 5531-5534.
27. Leidy, C., W. F. Wolkers, Jorgensen, K., Mouritsen, O. G. and Crowe, J. H., Biophys. J., **80**, (2001) 1819-1828.
28. Loura, L. M. S., Federov, A., and Prieto, M., Biophys. J., **80**, (2001) 776-788.
29. Buboltz, J. T. and Feigenson, G. W., Biochim. Biophys. Acta. **1417**, (1999) 232-245.
30. Drews, A. R., Barker, J. G., Glinka, C. J., and Agamalian, M., Physica B., **241-243**, (1998) 189-191.
31. Scherfeld, D., Kahya, N. and Schwille, P., Biophys. J., **85**, (2003) 37583768.
32. Kahya, N., Scherfeld, D., Bacia, K., and Schwille, P., J. Struct. Biol. **147**, (2004) 77-89.
33. Moody, M. F., Acta Cryst. **A31**, (1975) 815.
34. Stuhrmann, H.B., and Miller, A., J. Appl. Cryst. **11**, (1978) 325-345.
35. Mason, P.C., Gaulin, B.D., Epand, R.M., and Katsaras, J., Phys. Rev. E. **81**, (2000) 5634-5639.
36. Nayar, R., Hope, M. J., and Cullis, P. R., Biochim. Biophys. Acta. **986**, (1989) 200-206.
37. Ertel, A., Marangoni, A. G., Marsh, J. Hallett, F. R., and Wood, J. M., Biophys. J. **64**, (1993) 426-434.
38. Glinka, C. J., Barker, J. G., Hammouda, B., Krueger, S., Moyer, J. J., and Orts, W. J., J. Appl. Crystallogr. **31**, (1998) 430-440.
39. Kućerka, N., Nagle, J. F., Feller, S.E., and Balgavý, P., Phys. Rev. E., **69**, (2004) 051903-1051903-9.
40. Konarev, P. V., Volkov, V. V., Sokolova, A. V., Koch, M. H. J. and Svergun, D. I., J. Appl. Cryst. **36**, (2003) 1277-1282.
41. Sears, V. F., Neutron News, **3**, (1992) 26-37.
42. Nagle, J. F., and Tristram-Nagle, S. Biochim. Biophys. Acta, **1469**, (2000) 159-195.

43. Knoll, W., Schmidt, G., Ibel, K., and Sackmann, E., Biochemistry **24**, (1985) 5240-5246.
44. Hansen, S. J., Appl. Crystallogr. **23**, (1990) 344-346.
45. Henderson, S. J., Biophys. J. **70**, (1996) 1618-1627.
46. Pink, D. A., Merkel, R., Quinn, B. Sackmann, E. and Pencer. J., Biochim. Biophys. Acta. **1150**, (1993) 189-198
47. Pencer, J. and Hallett, F. R., Langmuir, **19**, (2004) 7488-7497.
48. Nieh, M.-P., Glinka, C. J., Krueger, S., Prosser, R. S., and Katsaras, J., Biophys. J., **82**, (2002) 2487-2498.
49. Gandhavadi, M., Allende, D., Vidal, A., Simon, S.A. and McIntosh, T.J., Biophys. J., **82**, (2002) 1469-1482.
50. Veatch, S. L. and Keller, S. L. Biophys. J., **84**, (2003) 725-726.
51. Knoll , W., Haas, J., Stuhrmann, H. B., Füldner, H.-H., Vogel, H., and Sackmann, E., J. Appl. Cryst. **14**, (1981) 191-202.